The single-cell chemostat: an agarose-based, microfluidic device for high-throughput, single-cell studies of bacteria and bacterial communities

Lab on a Chip

Dynamic Article Links ►

Cite this: DOI: 10.1039/c0xx00000x

www.rsc.org/xxxxxx

PAPER

The single-cell chemostat: an agarose-based, microfluidic device for high-throughput, single-cell studies of bacteria and bacterial communities

Jeffrey R. Moffitt, [‡a] Jeffrey B. Lee,[‡b] and Philippe Cluzel[a,b,c]

Received (in XXX, XXX) Xth XXXXXXXXX 20XX, Accepted Xth XXXXXXXXX 20XX
DOI: 10.1039/b000000x

Optical microscopy of single bacteria growing on solid agarose support is a powerful method for studying the natural heterogeneity in growth and gene expression. While the material properties of agarose make it an excellent substrate for such studies, the sheer number of exponentially growing cells eventually overwhelms the agarose pad, which fundamentally limits the duration and the throughput of measurements. Here we overcome the limitations of exponential growth by patterning agarose pads on the sub-micron-scale. Linear tracks constrain the growth of bacteria into a high density array of linear micro-colonies. Buffer flow through microfluidic lines washes away excess cells and delivers fresh nutrient buffer. Densely patterned tracks allow us to cultivate and image hundreds of thousands of cells on a single agarose pad over 30-40 generations, which drastically increases single-cell measurement throughput. In addition, we show that patterned agarose can facilitate single-cell measurements of bacterial communities. As a proof-of-principle, we study a community of *E. coli* auxotrophs that can complement the amino acid deficiencies of one another. We find that the growth rate of colonies of one strain decreases sharply with the distance to colonies of the complementary strain over distances of only a few cell lengths. Because patterned agarose pads maintain cells in a chemostatic environment in which every cell can be imaged, we term our device the single-cell chemostat. High-throughput measurements of single cells growing chemostatically should greatly facilitate the study of a variety of microbial behaviours.

Introduction

The behaviours of individual bacteria often differ from those of the average population. Individual cells display broad distributions of growth rates and gene expression[1], adopt rare, but often clinically relevant, phenotypes[2, 3], and display oscillatory behaviours that are not synchronized across the population[4]. In parallel, recent studies have illustrated that sub-populations of cells within microbial communities can play important roles in the dynamics of the community[5]. In a natural setting, bacteria often exist as members of complex communities, in which, small molecule exchange drives a variety of emergent phenomena, such as quorum sensing[6], cell differentiation[5], antibiotic resistance[7], symbiosis[8], and territoriality[9]. Unfortunately, the single-cell origins of these bacterial phenomena have yet to be understood.

High-resolution, time-lapse microscopy of single growing cells is one of the most powerful techniques for studying the behaviours of single bacteria[1]. In typical measurements, cells are placed on a flat substrate and imaged repeatedly as they grow. For the last century, agar or agarose gels have been the substrate of choice for these measurements[1]. Agarose is soft, porous and transparent. Thus, minimal pressures hold cells in place for repeated imaging; nutrients are diffusively replenished from nutrient stored in the bulk of the gel; and cells can be easily imaged with the full range of fluorescent and non-fluorescent imaging modalities[1].

However, agarose gels have limitations that restrict the range of biological questions that can be addressed with time-lapse imaging. Left unchecked, cell number increases exponentially and cells eventually overwhelm the agarose pad (Fig. 1a). Consequently, multiple layers of bacteria form, preventing the imaging of individual cells. Nutrient consumption eventually out-competes diffusion, producing a chemical environment that is not constant in space or time. Finally, exponential growth amplifies minute differences in growth rate into large changes in the composition and spatial arrangement of the bacterial community (Fig 1a.), complicating quantitative measurements of cell-to-cell communication within mixed bacterial communities.

Several recent microfluidic devices have been introduced to address these problems[10-16]. By patterning surfaces on the cellular-scale, growing cells are corralled within small tracks or cavities that limit crowding and produce spatially organized communities of bacteria of fixed density. However, the typical material used to fabricate these devices, polydimethylsiloxane (PDMS), has some potential drawbacks when compared to agarose that may limit the applicability of these devices. First,

PDMS is relatively stiff[17], and even slightly undersized PDMS cavities can introduce severe mechanical stress to cells[18]. Second, PDMS is less permeable to aqueous solutions than agarose[17], and a small number of cells can deplete the local nutrient environment over surprisingly small distance scales—a few cell lengths[15, 16]. Moreover, this limited permeability may inhibit the small molecule exchange responsible for cell-to-cell communication. Third, with a relatively large index of refraction, PDMS is not always imaging-friendly, and in some circumstances, fluorescent contrast agents are required to visualize cells[11, 12]. Finally, uncured PDMS can leach from structures and accumulate in growing cells with unknown biological effects[19].

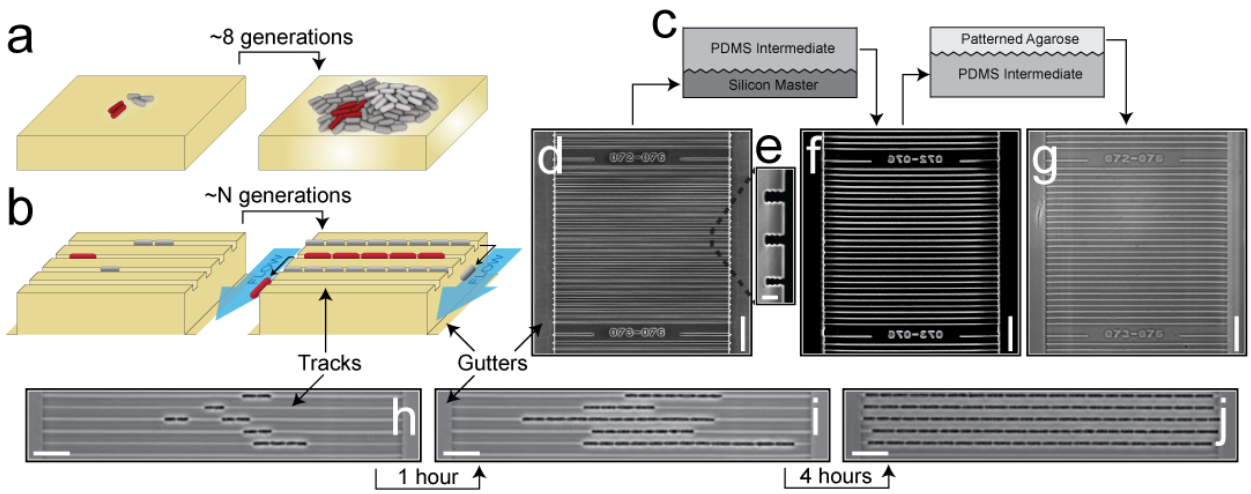

Fig. 1 Patterned agarose directs bacterial colony growth. (a) Bacterial crowding on an agarose pad. Multiple layers of cells prevent individual-cell imaging, nutrient consumption out-competes diffusion, producing spatiotemporal nutrient changes, and imbalanced growth changes the community composition and spatial arrangement. Because of these limitations, most measurements are not reported beyond 6-8 generations[1]. (b) Patterned agarose corrals cells into defined tracks. (c) Construction of a patterned agarose pad. (d) Scanning electron micrograph (SEM) of a silicon master. (e) SEM of the track profile. (f) SEM of a PDMS intermediate. (g) Phase contrast image of a patterned agarose gel. (h –j) Phase contrast images of *E. coli* growing on a patterned gel. Scale bars are 20 μm in panels (d), (f), and (g), 1 μm in panel (e), and 10 μm in panels (h), (i) and (j).

Here we introduce a microfluidics platform for single-cell studies that combines the benefits of structured surfaces with those of biologically and imaging friendly agarose, circumventing the potential limitations of PDMS. We pattern agarose pads on the sub-micron-scale to create a platform in which (i) single-cells can be imaged directly with a variety of imaging modalities, (ii) the nutrient environment is spatially homogeneous and constant in time, (iii) bacterial colonies are spatially organized at high density, (iv) multiple bacterial strains can be cultivated simultaneously, and (iv) small molecule exchange within spatially-organized, mixed communities of bacteria is maintained. Because our structured agarose pad maintains complex communities of bacteria in constant nutrient environments in which every cell can be imaged individually, we refer to our structured agarose pad as a *single-cell chemostat*.

Experimental

Fabricating Patterned Agarose Pads

We created two basic structures in agarose pads to control cell crowding and density. Sub-micron *tracks* confined cells and directed their growth into linear colonies that terminate in *gutters*. Buffer flow through the gutters washed away excess cells pushed from the tracks, and it also delivered fresh nutrient locally, which supported the uniform growth of a high density array of cells (Fig. 1b).

We followed a three-step lithographic process to fabricate agarose pads with sub-micron structured surfaces (Fig 1c). First, we created silicon masters containing the positive of the desired features. We performed two rounds of photolithography[17] to create, first, the smaller tracks and then, second, the larger gutters (Fig. 1d; Fig. S1). To fabricate tracks with widths narrower than the diffraction limit of our etching process, we used chemical vapor deposition to deposit 100-nm to 300-nm thick layers of SiO_2 after etching. All track dimensions were confirmed with scanning electron microscopy (Fig. 1d&e). To probe the appropriate range of track sizes for directing cellular growth, each silicon wafer contains tracks with three different widths (Fig. 1e). In addition, we have created wafers with tracks that cover a range of dimensions, widths from 300 nm to 1.0 μm, depths from 0.75 to 1.5 μm, and lengths from 50 to 200 μm (Figs. S1 & S2). Tracks were grouped into labelled 100-μm blocks, allowing each of the approximately 100,000 tracks on a single 1.5-cm-square print to be uniquely identified.

We then created negative molds of the silicon masters by replicating them into PDMS intermediates (Fig. 1f). To avoid the lateral collapse of high aspect ratio tracks[17], we employed solvent assisted[20], composite PDMS molding to create a layer of hard PDMS[21] containing our features supported by a soft PDMS backing[17, 20-22]. We utilized PDMS intermediates for two reasons. First, the decrease in track dimensions with the addition of SiO_2 layers required a positive silicon master. Second, we found that the PDMS intermediates can be used repeatedly without damage. Thus, the inexpensive PDMS intermediates prolong the life of the expensive silicon masters by removing them from day-to-day use.

To cast PDMS intermediates, cleaned wafers were silanized (tridecafluoro-1,1,2,2-tetrahydrooctyl-1-trichlorosilane; T2492, United Chemical Technology) using standard protocols[17]. h-PDMS[21] (13.6 g 8% vinyl-methylsiloxane-dimethyl-siloxane; VDT-731, Gelest; 72 μL platinum divinyl-tetramethyl-disiloxane;

SIP6839.3, Gelest; 0.4 g 2,4,6,8-tetramethyl-tetravinyl-cyclotetrasiloxane; 87927, Sigma-Aldrich; 4 g 25-30% methylhydrosilxane-dimethylsiloxane ;HMS-H271, Gelest; and 2 g of hexane) was degassed for 5 minutes under house vacuum. An initial slow spin (100 rpm, 10s) created a thick layer of h-PDMS, which was then degassed for 5 minutes to ensure that all features were filled. A second spin (500 rpm, 5 s; 1000 rpm, 40s) created the final thin layer. The coated wafer was cured at 60C for 1 hour before a thick layer (~3-5 mm) of Sylgard 184 (10:1 ratio; Ellsworth Adhesives) was added. The composite print was cured at 60°C overnight and then gently removed from the silicon master.

Finally, we created patterned agarose pads by casting low-melting point agarose (BP165, Fisher Scientific) on the PDMS intermediates. To aid in the wetting of the PDMS intermediates by the molten agarose, the PDMS intermediates were either pretreated with O_2 plasma (Harrick Plasma; 18W, 3 s, 1000 mTor atmosphere) or chilled to 12°C. Gels were cast slowly in a warm room (30°C; 40% relative humidity), and high fidelity features were printed after 1 hour. Phase contrast images of printed agarose (Fig. 1g and Fig. S2) confirmed that the tracks and gutters were transferred to agarose with high fidelity. Once cast, gels could be soaked for days in aqueous media either for storage or to introduce temperature sensitive buffers, e.g. antibiotics. Used PDMS intermediates were washed in a 90°C deionized water bath and showed no damage from repeated printing. Wetting of the PDMS surfaces improved with repeated printing. Using these methods, we could produce high quality prints of tracks as narrow as 300 nm (Fig. S2). Similar methods have been used to print tracks of 2-μm width[23, 24]. Thus, our results indicate that the lithographic limit of agarose is almost an order of magnitude smaller than previously demonstrated.

Experiment Assembly.

We have designed a custom sample chamber to introduce buffer to the gutters and to prevent gels from drying (Fig. S3). Briefly, gel chambers were created by plasma bonding (18W, 20 s, 1000 mTor atmosphere) glass cover slips to PDMS sidewalls (Fig. S3f). PDMS sidewalls contained a cavity similar in size to the cast gel but slightly undersized (~5%) in width and height. The compression needed to fit the gel into the undersized chamber insured that i) cells are held firmly in place on the bottom cover glass and ii) buffer must flow through gutters not around the gel. To assemble an experiment, the sample chamber was plasma treated to activate the surface (as above), 1 μL of cell culture was added to the chamber, and the patterned agarose pad was pressed into place. The chamber was sealed with the addition of a second, plasma-treated coverslip. The plasma bond was allowed to set for 15 minutes before buffer was introduced into the device. A 30G needle inserted into the front buffer reservoir removed trapped air as buffer was introduced and was removed once the fluidic line was filled. A syringe pump (KDS-210, KD Scientific) provided continuous buffer flow through the device (0.5 – 30 μL/min). A fully assembled experimental chamber is pictured in Figure S3.

Strains and Growth Conditions.

E. coli growth experiments were conducted with MG1655 containing a low copy plasmid conferring ampicillin resistance (gift of A. Subramaniam). *E. coli* community experiments were conducted with strains from the Keio knockout library[25] supplemented with a plasmid expressing a fluorescent marker[26] (gift of J. Wintermute and P. Silver.) MG1655 with a GFPmut2 and a kanamycin cassette introduced at the lambda integration site was used as the prototroph. *B. subtilis* growth experiments were conducted with strains PY 79 (gift of B. Burton) and 3610 (gift of T. Norman and R. Losick). All reported data are from 3610. *E. feacalis* measurements were conducted with strains, V583 and E1sol (gift of M. Gilmore). All reported data are from E1sol.

E. coli experiments were conducted with either rich or minimal MOPS defined media (Teknova) with either 0.2% w/v glucose or 0.2 % w/v glycerol supplemented with 0.002% v/v Tween20. *B. subtilis* and *E. feacalis* measurements were conducted with LB and brain heart infusion (BHI), respectively. When appropriate, buffers were supplemented with either 50 μg/ml ampicillin or 10 μg/mL kanamycin. For general growth measurements, cells were harvested at an OD_{600} of 0.2 from cultures diluted 1/1000 from overnight cultures.

For community experiments, the auxotrophs were harvested from amino-acid-limited overnight cultures in minimal media supplemented with either 50 μM arginine or 42 μM isoleucine, leucine, and valine. Cells were mixed in the desired ratio, washed once with amino acid free media, and concentrated 5-fold. Gels were cast with deionized water and soaked overnight in the same MOPS minimal medium supplemented with 10 μM of arginine, isoleucine, leucine, and valine. After 5 hours of growth on the necessary amino acids, 12 hours of 10 μL/min flow of amino acid free MOPS minimal medium removed these amino acids.

Time-lapse Imaging.

Most time-lapse movies were collected on a home-built phase-contrast microscope incorporating an LED illumination source, a 100X, 1.49NA objective (Nikon), an external PH4 ring and annulus (Nikon), and a micro-lensed CCD camera (Alta-U32, Apogee, Inc.) Samples were positioned with a two-axis micropositioner (MicroStage-5E, Mad City Labs). The microscope was automated using custom LabView software (National Instruments). Sample temperature was maintained at 35°C by heating the objective with a custom-built heating stage. Measurements of 200-μm long colonies were conducted on a Zeiss Axiovert 200M with a 20x, 0.8 NA, apochromat, phase-contrast objective, a PH2 annulus, and a cooled CCD camera (C4742-98, Hamamatsu). The temperature was held at 37°C with a microscope enclosure. All time-lapse movies were collected with 1 minute resolution, unless otherwise noted.

Image Analysis.

All image analysis was performed with custom software written in Matlab (MathWorks). Frames were aligned using image correlation and sub-images of the labels. Individual colonies were cropped and subsequent frames combined to form a single, kymograph-like composite image. Individual frames were filtered with a Laplacian of a Gaussian to remove noise and background variations, and Otsu's method was used to pick the threshold for creating a binary image. Binary images were then eroded with a 2 pixel circular disk to accentuate forming septa, and connected regions within the final binary images, i.e. cells, were identified. Cells in one frame were identified in subsequent frames by

predicting their new locations given the center velocity for cells at a given position averaged over the dynamics of the entire colony in the previous five frames. Errors were occasionally introduced during cell segmentation and were manually corrected. Lineage construction, on the other hand, was fully automated and required no user intervention. The robustness of lineage construction originates from the simple and strict relationship between inheritance and position in the colony and represents a significant advantage of growth in linear colonies over growth in unstructured, two-dimensional colonies.

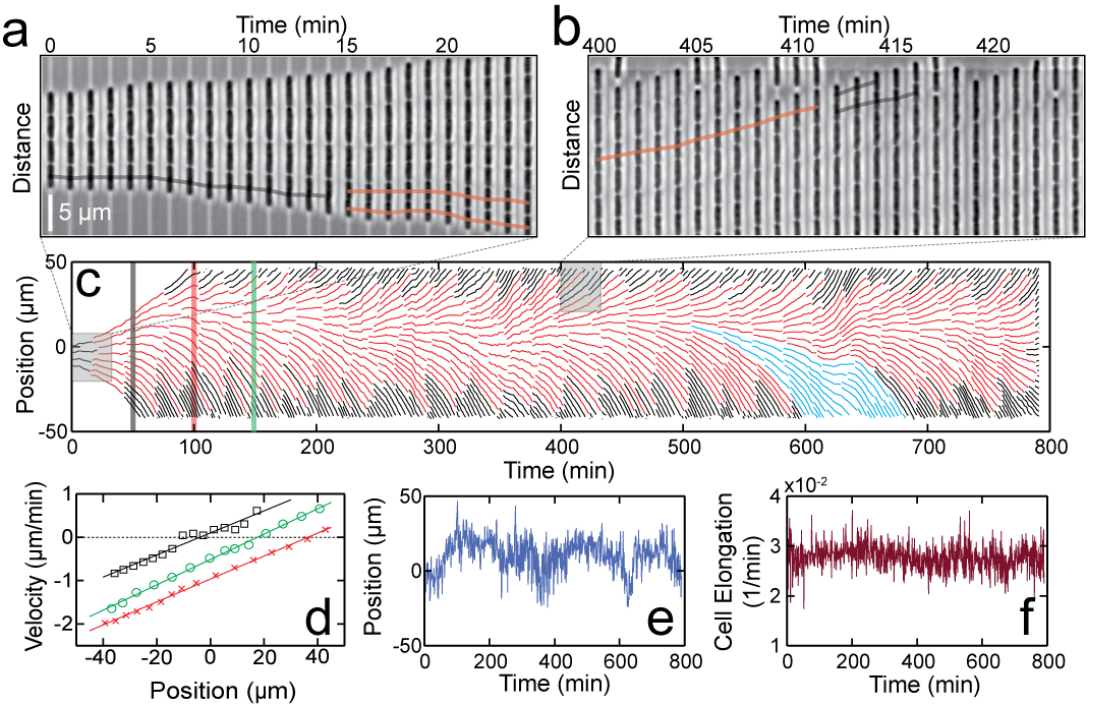

Fig. 2 Cellular growth on patterned agarose. (a) Kymograph-like, phase-contrast image of *E. coli* growing in a 0.6x1.5x100-μm track in rich defined medium at 35°C. Each sub-image is a subsequent frame from a time-lapse movie. Solid lines represent the motion of a cell and its daughters. (b) Kymograph-like, phase contrast image from the same colony, approximately 6 hours later showing cells being pushed into the gutters. A subset of the cellular lineages are marked (colored lines) in (a) and (b). (c) Center position of every cell in this colony as a function of time. Cells for which both the initial and final division have (red) or have not (black) been observed are plotted. To illustrate lineage motion within the colony, one lineage of cells is specifically marked (blue). (d) The center velocity versus the position within the track for cells from different times (marked with colored bars in (c)). The solid lines are linear fits. (e) The stationary position of the colony (the zero crossing in panel (d)) as a function of time. (f) The slope of cell velocity versus position as a function of time. This slope is equivalent to the average fractional elongation of the cells within the colony. The scale bars in (a) and (b) are 5 μm.

SEM Imaging.

All scanning electron microscopy (SEM) images were collected with a Supra55VP (Zeiss). The top and side view images presented in Figure 1 were collected with the InLens detector while the angled views in Figure S1 were collected with the SE2 detector. Since PDMS is non-conductive and charges under high vacuum SEM imaging, we collected images of the intermediates using the variable pressure mode of the Supra55VP with a pressure of 16 Pa and the variable pressure detector with a bias of 380V. All images were collected with a 10 keV beam energy.

Results and Discussion

Bacterial Growth in the Single-Cell Chemostat.

We first probed the suitable range of track dimensions to confine and direct growing *E. coli*. We deposited cells on a printed gel, enclosed the gel in a custom chamber, flowed rich medium through the gutters, and collected time-lapse, phase contrast movies (Experimental Methods; Fig. S3). For a wide range of track sizes, we found that *E. coli* spontaneously aligned with the tracks, and, as cells divided, they grew within the tracks to form linear colonies. Over a few hours, the tracks filled and excess cells were pushed into the gutters and washed away (Figs. 1h-j, 2a&b, Movie S1). Because the agarose is not chemically bound to the glass, cells can occasionally lift the agarose and grow to form two dimensional, unstructured colonies. However, when the tracks are deeper (1.0, 1.25, and 1.5 μm) but narrower (0.3 – 0.8 μm) than the diameter of *E. coli* (roughly 0.8 μm in the rich medium of these measurements), we find that the vast majority of colonies are confined within the tracks (see, for example, Movie S1.) In addition, shorter tracks (50 and 100 μm) produced confined colonies more frequently than longer tracks (150 and 200 μm), though individual colonies as long as 0.4 mm were observed on gels fabricated without gutters.

Next, to characterize the growth of cells on patterned agarose, we used custom image analysis software to identify individual cells and reconstruct cellular lineages from time-lapse movies (Fig. 2a-c; Materials and Methods). We found that the rate at which cells were pushed towards the gutters increased proportionally to the distance from a position near the center of the colony (Fig. 2d). However, because all of the cells are free to move within the tracks, the position of this 'source' position changes in time (Fig. 2e). Finally, we found that the rate at which

cells move outward as a function of distance (the slope in Fig. 2d) is constant in time (Fig. 2f). This rate corresponds to the average fractional elongation rate of the cells within the colony; thus, cellular growth is constant across the roughly 30 generations of Figure 2. This observation indicates that the buffer flow in the gutters was sufficient to maintain a chemostatic environment. Additionally, we found that the growth properties of individual cells, e.g. the division time, the average elongation rate, and the length at division, were also constant throughout this measurement (Fig. S4).

To confirm that cellular growth is not perturbed on patterned agarose, we measured the growth of *E. coli* as a function of the track width and agarose stiffness. We found that cellular growth does not depend on either of these parameters (Fig. S5); thus, the pressure required to confine cells within tracks does not perturb their growth. In addition, we grew cells in tracks 200 μm in length to probe for position-dependent growth effects. We did not find a position-dependence to growth (Fig. S6), confirming i) that the pressure required to push out cells does not perturb growth and ii) that diffusive transport through the gel maintains a spatially uniform nutrient environment over distances of at least 100 μm. Finally, we found that the average growth rates observed on structured agarose agree with those measured in bulk culture at the same temperature and with the same growth medium (data not shown).

Because there is a range of acceptable track sizes that can confine growing E. coli, we reasoned that identical tracks might deform to fit a range of bacterial sizes and morphologies. To test this hypothesis, we first cultivated *E. coli* under a range of nutrient conditions known to decrease cell size[27]. Figure 3 and Movies S1-S3 show that identical tracks confined *E. coli* under all tested nutrient conditions. Using the same track sizes, we also cultivated the gram-positive, rod-shaped bacteria, *B. subtilis*, and a gram-negative, spherical bacteria, *E. faecalis*. Figure 3 and Movies S4 and S5 revealed that tracks of identical width and depth deformed appropriately to confine these bacteria despite their different morphologies. The cyanobacteria, *S. elongatus*, could also be grown in identically sized tracks (S. W. Teng and E. O'Shea, personal communication). To confirm that unperturbed growth in the confined environment of the tracks is not specific to *E. coli*, we repeated control experiments with *B. subtilis* and found that the growth of this bacterium is also not perturbed on patterned agarose (Figs. S5-S7). Finally, in PDMS-based devices aberrant cellular morphologies were observed when cells exited small constrictions[18]. By contrast, in our agarose-based device, we show that cells exiting the tracks have morphology indistinguishable from cells still within the tracks (Fig. 3c). Thus, soft agarose tracks are 'one-size-fits-all,' conforming to different bacterial sizes while not perturbing the growth of the confined bacteria.

Finally, the density of printed tracks substantially increased measurement throughput over that reported for conventional agarose pads. For example, consider the 100x100-μm field of view of Movie S1. A modest filling of the tracks produced 20 colonies in this field of view, and throughout a single overnight measurement, 30 generations and the full division cycle of roughly 10,000 cells were measured. By contrast, measurements

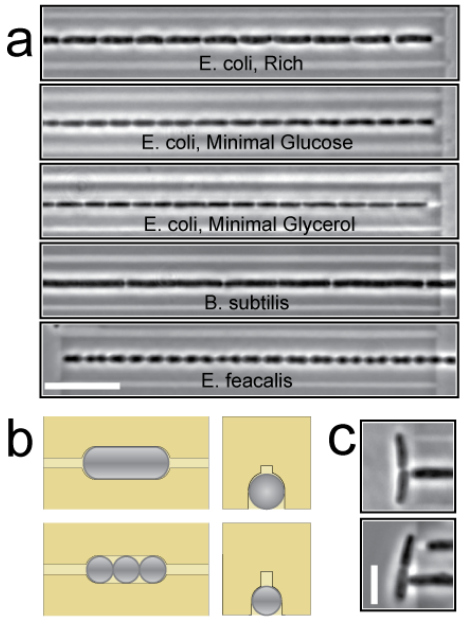

Fig. 3 Soft agarose tracks accommodate a range of bacterial morphologies. (a) Phase contrast images of *E. coli* in rich defined medium (first from top), *E. coli* in minimal defined medium with glucose (second from top), *E. coli* in minimal defined medium with glycerol (third from the top), *B. subtilis* in LB (second from bottom), and *E. faecalis* in BHI (bottom). Despite their different morphologies all of these bacteria are confined with 1.5-μm deep tracks ranging from 0.6 – 0.8-μm in width. (b) Cartoon depiction of the ability of agarose tracks to deform to fit a wide variety of bacterial morphologies. (c) Phase-contrast images of *E. coli* temporarily stuck to the coverglass after being expelled from the tracks. The scale bar is 10 μm in (a) and 3 μm in (c).

of two dimensional colonies growing on conventional agarose pads are typically not reported beyond 8 generations (256 cells), and only 1-2 such colonies would fit in a similar field of view[1]. Thus, structured agarose increases single-cell measurement throughput by nearly two orders of magnitude, producing comparable if not slightly more single-cell measurements per frame than the highest throughput PDMS-based devices[12]. Moreover, this high throughput is achieved while maintaining the beneficial properties of unstructured agarose: a uniform nutrient environment, applied pressures that are non-perturbative for growth, and applicability to a variety of bacterial species.

Growth of Mixed Microbial Communities in the Single-Cell Chemostat.

With the ability to confine a variety of bacteria with agarose tracks of identical width, it should be possible to cultivate spatially organized, mixed microbial communities in the single-cell chemostat with small-molecule exchange facilitated by the porous walls that separate colonies. To test this possibility, we studied a recently discovered, synthetic microbial community composed of *E. coli* auxotrophs. In particular, we studied the interaction of ΔilvE, a strain deficient in isoleucine and valine synthesis, with ΔargC, a strain deficient in arginine synthesis. Previous bulk co-culture[28] has established that each of these strains cannot grow alone in amino-acid free medium, but when co-cultured, they share the needed metabolites, and both strains grow. We chose this system because the growth rate of these strains provides a direct, quantitative measure of the interaction

between the two strains.

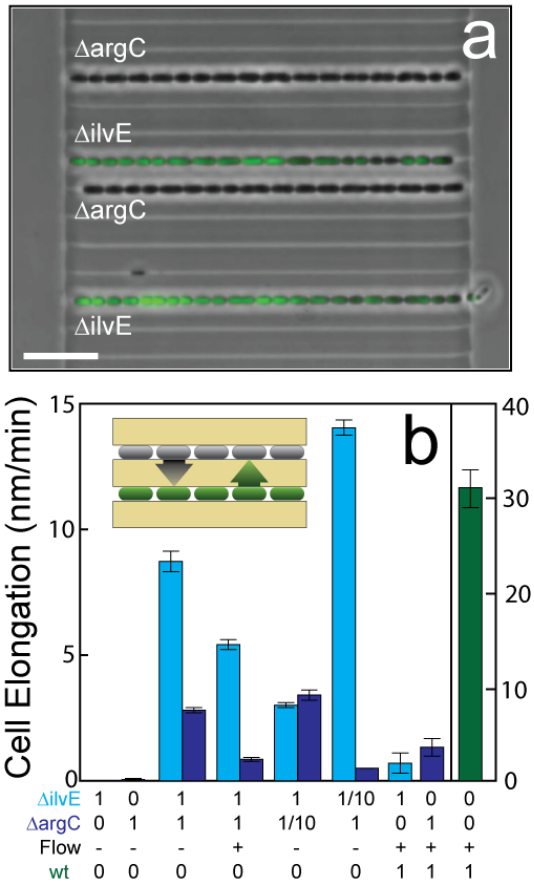

Fig. 4 Growing spatially-defined, chemostatic bacterial communities with patterned agarose. (a) Combined phase-contrast (gray) and fluorescence image (green) of a mixed microbial community consisting of two *E. coli* auxotrophs, ΔilvE (green) and ΔargC (gray). The scale bar represents 10 μm. (b) Average cell elongation rate for ΔilvE (cyan), ΔargC (purple), and wild-type prototrophic (green) colonies as members of communities of different composition, under conditions of gravity flow (-), or 10 μL/min (+) or 5 μL/min (auxotroph-prototroph experiments) flow. Unit concentration corresponds to roughly 1 colony per 5 tracks. Error bars correspond to standard error. Inset: cartoon depiction of colonies communicating via small molecule exchange through the surrounding gel.

To create a microbial community with these auxotrophic strains, we combined them in various proportions, plated the mixture on patterned agarose, assembled the gel within our custom sample holder, and allowed the community to grow in the presence of all of the needed amino acids (Materials and Methods; Fig. S8). Once the community was established, amino acids were washed away, and the growth of each strain was measured. We found that communities composed of only one auxotroph did not grow once the needed amino acids were removed. But a mixed community with equal numbers of each strain did grow (Fig. 4), indicating that i) the necessary nutrients are made and shared by surrounding cells and ii) the modest buffer flow required to maintain chemostatic growth of the community does not suppress complementation. Increasing the rate of buffer flow through the gutters decreased the growth rate

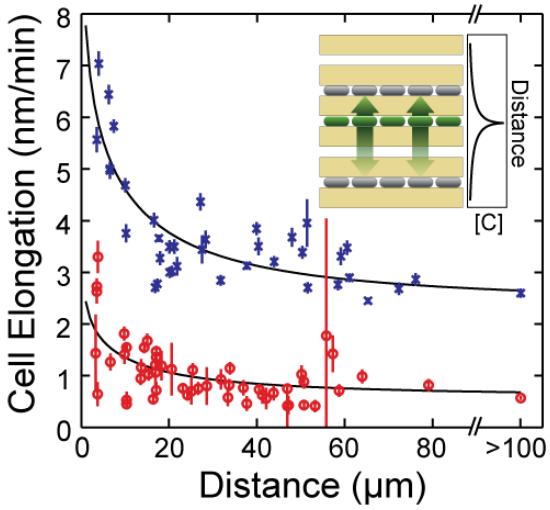

Fig. 5 Patterned agarose reveals distance-dependent communication. Average cell elongation rate for ΔilvE colonies as a function of the distance to the nearest ΔargC colony for communities composed of 1/10 ΔargC (purple) or 1/30 ΔargC (red) and for ΔilvE from 100-μm fields of view in which no ΔargC colonies were present (>100). Error bars represent standard deviation. Solid lines correspond to fits to the expected growth rate from a concentration gradient established from a line source when growth is linear in the concentration of the necessary metabolite: $a\,\mathrm{csch}^{-1}(2y/L)+g_0$, where y is the separation between colonies, L is the 50-μm length of the colony, and g_0 is the observed growth when ΔilvE colonies are further than 100 μm from the nearest ΔargC colony. The scaling parameter a is the only free parameter (See SI Discussion). Inset: cartoon depiction of the expected concentration profile created by a single ΔargC colony (green) and observed by different ΔilvE colonies (gray).

of both strains, consistent with an increased dilution of the shared metabolites (Fig. 4b). Similarly, decreasing the abundance of one strain decreased the growth rate of the other (Fig. 4b), again confirming that the necessary metabolites are generated by the complementary strain. Moreover, despite large differences in growth rates between the two strains, the composition of the community, and, thus, the growth rate of each strain was constant in time (Fig. S8).

The ability to reconstitute a microbial community with a stable composition in a chemostatic environment in which every cell can be directly imaged allowed us to address questions that would be difficult or impossible to answer with bulk co-culture measurements. For example, we first asked whether the auxotrophic state was necessary for complementation. To probe this question we created mixed communities of wild type *E. coli*, capable of making all of the needed amino acids, with each of the auxotrophs individually. The significant growth advantage of the wild type cells over the auxotrophs would make this measurement difficult in bulk co-culture since the wild type cells would quickly overwhelm the culture. However, despite nearly two orders of magnitude difference in growth rate between the wild type cells and each of the auxotrophs (Fig. 4b), we found that patterned agarose maintained a stable community composition (Movie S7). The auxotrophs grew in the presence of wild type *E. coli*, indicating that the auxotrophic state is not required for the sharing of metabolites.

Next, we asked whether all cells were growing within the mixed community or if a sub-population of cells produced the observed average growth. We computed the distribution of cell elongation rates for individual cells from a community composed

of equal numbers of each of the auxotrophs and found that all cells were growing with a broad distribution of rates (Fig. S9). Moreover, while daughter cells did inherit their growth rate from mother cells, this correlation was lost by the next generation (Fig. S9). Thus, we concluded that while some cells can transiently exploit this emergent symbiosis to a greater degree, all cells within the community are capable of growing in the presence of the shared metabolites.

Finally, we asked whether the strength of the complementation had a proximity-dependence. In other words, do complementary colonies closer to one another grow faster than colonies separated by larger distances? To address this question, we quantified the growth of ΔilvE colonies as a function of distance to the nearest ΔargC colony for fields of view in which only one ΔargC colony was present (Fig. 5). For communities containing either 1/10 or 1/30 ΔargC relative to ΔilvE, we found that ΔilvE colonies within a few tracks, ~20 μm, of a ΔargC colony grew significantly, 3-5 fold, faster than colonies separated by larger distances. Colonies that were separated by large distances continued to grow, experiencing an average low metabolite concentration that is lowered by decreasing the fraction of ΔargC. Thus, in this spatially organized community, complementation is significantly enhanced between communities separated by only a few cell lengths.

Proximity-dependent communication has been observed previously in microbial communities with the aid of microfluidic devices[29, 30]. However, in these measurements the strength of the communication between complementary strains decreased over distance scales of several hundred microns—nearly an order of magnitude larger than the distances we observe. To rationalize this difference, we considered a simple production-diffusion model in which a linear colony acts as a line source of nutrient (Fig.5, Supplemental Discussion). In strict analogy to the voltage produced by a line source, we find that the absolute concentration of shared metabolites is set by the production rate of these metabolites (the electric charge) and their diffusion constant (the permittivity) but that the distance scale over which the concentration decays is set only by the geometry of the source. In previous work, distinct species were 100s of microns in dimension[29, 30], whereas colonies within the single-cell chemostat were only 50-microns long; thus, concentration profiles produced by our strains should decay over shorter distances. Our measurements confirm that spatial structure on the cellular-scale can play a dramatic role in regulating the interaction between strains within mixed microbial communities, highlighting the potential importance of controlled cellular-scale geometries in the study of cell-to-cell communication.

Conclusions

Time-lapse microscopy of bacterial cells growing on solid agar or agarose support has been a tremendously successful technique in microbiology. Here we have addressed one of the limitations of this technique—the unrestricted exponential growth of cells—by patterning agarose pads on the sub-micron scale with soft lithographic methods. We have shown that patterned agarose pads (i) direct the growth of high density, linear colonies without perturbing the growth of cells, (ii) maintain a spatially uniform, chemostatic environment, (iii) preserve small molecule exchange between colonies, and (iv) allow each cell to be individually addressed and imaged with both phase and fluorescence modalities. By using agarose rather than the more common microfluidic material, PDMS, we have avoided potential problems due to mechanical stress, non-uniform nutrient environments, and restricted small molecule exchange. Thus, we have combined the established benefits of structured surfaces with those of agarose. For this reason, the agarose-based single-cell chemostat may represent a useful alternative to existing microfluidic devices[10-16] for high-throughput, single-cell measurements of bacteria. When combined with the success of several additional hydrogel-based microfluidic devices designed for cell culture[31, 32], our results indicate the potential benefits of agarose and other hydrogels for the construction of biologically friendly microfluidic devices.

In addition, we have shown that the single-cell chemostat can be used to create chemostatic, bacterial communities—mixed communities of fixed composition growing in a constant nutrient environment. Soft agarose tracks deform to fit bacteria of different sizes and morphologies, allowing multiple strains to be simultaneously cultivated within the same microfluidic device. Moreover, because the walls that physically separate adjacent colonies are porous, small molecule exchange between these colonies is preserved. Thus, the single-cell chemostat can be used to both control the local spatial structure and study its effect on intercellular communication. A variety of remarkable bacterial behaviours emerge only within a community setting, and the single-cell chemostat may be a powerful tool for dissecting the single-cell origins of these behaviours.

Acknowledgements

We thank L. Bruneaux, C. Guet, and L. Chomaz for preliminary work; M. Kim, E. Balleza, A. Subramaniam, S. Nishida, S. Jun, and L. Robert for technical advice; J. Su, L. David, K. Dave, and the Cluzel laboratory for a critical reading of the manuscript; and the laboratories of M. Gilmore, P. Silver, B. Burton, R. Losick, and K. Gibbs for strains. We thank DiCon Fiberoptics Inc. for technical advice and for all micro-fabrication. J.R.M. was funded by the Helen Hay Whitney Foundation. This work was performed in part at the Center for Nanoscale Systems (CNS), a member of the National Nanotechnology Infrastructure Network (NNIN), which is supported by the National Science Foundation under NSF award no. ECS-0335765. CNS is part of Harvard University. This research was partly funded by NIH grant P50GM081892 to the Systems Biology Center at the University of Chicago (to P.C.).

Notes and references

[a] *Center for Systems Biology, Harvard University, Cambridge, MA.*
[b] *School of Engineering and Applied Sciences, Harvard University, Cambridge, MA.*
[c] *Department of Molecular and Cellular Biology, Harvard University, Cambridge, MA. Email: cluzel@mcb.harvard.edu;Tel: 617-495-8745.*

† Electronic Supplementary Information (ESI) available. See DOI: 10.1039/b000000x/
‡ These authors contributed equally.

1. J. C. W. Locke and M. B. Elowitz, *Nat Rev Micro*, 2009, **7**, 383-392.

2. J.-W. Veening, W. K. Smits and O. P. Kuipers, *Annual Review of Microbiology*, 2008, **62**, 193-210.
3. O. Gefen and N. Q. Balaban, *Fems Microbiology Reviews*, 2009, **33**, 704-717.
4. J. C. W. Locke, J. W. Young, M. Fontes, M. J. H. Jiménez and M. B. Elowitz, *Science*, 2011, **334**, 366-369.
5. H. Vlamakis, C. Aguilar, R. Losick and R. Kolter, *Genes Dev*, 2008, **22**, 945-953.
6. C. M. Waters and B. L. Bassler, *Annual Review of Cell and Developmental Biology*, 2005, **21**, 319-346.
7. H. H. Lee, M. N. Molla, C. R. Cantor and J. J. Collins, *Nature*, **467**, 82-85.
8. E. H. Wintermute and P. A. Silver, *Genes & Development*, 2010, **24**, 2603-2614.
9. K. A. Gibbs, M. L. Urbanowski and E. P. Greenberg, *Science*, 2008, **321**, 256-259.
10. M. R. Bennett and J. Hasty, *Nat Rev Genet*, 2009, **10**, 628-638.
11. N. Q. Balaban, J. Merrin, R. Chait, L. Kowalik and S. Leibler, *Science*, 2004, **305**, 1622-1625.
12. P. Wang, L. Robert, J. Pelletier, W. L. Dang, F. Taddei, A. Wright and S. Jun, *Current Biology*, 2010, **20**, 1099-1103.
13. A. C. Rowat, J. C. Bird, J. J. Agresti, O. J. Rando and D. A. Weitz, *Proc Natl Acad Sci U S A*, 2009, **106**, 18149-18154.
14. D. Di Carlo, L. Y. Wu and L. P. Lee, *Lab on a Chip*, 2006, **6**, 1445-1449.
15. W. Mather, O. Mondragon-Palomino, T. Danino, J. Hasty and L. S. Tsimring, *Physical Review Letters*, 2010, **104**, -.
16. H. J. Cho, H. Jonsson, K. Campbell, P. Melke, J. W. Williams, B. Jedynak, A. M. Stevens, A. Groisman and A. Levchenko, *Plos Biology*, 2007, **5**, 2614-2623.
17. D. Qin, Y. Xia and G. M. Whitesides, *Nat. Protocols*, 2010, **5**, 491-502.
18. J. Mannik, R. Driessen, P. Galajda, J. E. Keymer and C. Dekker, *PNAS*, 2009, **106**, 14861-14866.
19. K. J. Regehr, M. Domenech, J. T. Koepsel, K. C. Carver, S. J. Ellison-Zelski, W. L. Murphy, L. A. Schuler, E. T. Alarid and D. J. Beebe, *Lab on a Chip*, 2009, **9**, 2132-2139.
20. H. Kang, J. Lee, J. Park and H. H. Lee, *Nanotechnology*, 2006, **17**, 197-200.
21. T. W. Odom, J. C. Love, D. B. Wolfe, K. E. Paul and G. M. Whitesides, *Langmuir*, 2002, **18**, 5314-5320.
22. H. Schmid and B. Michel, *Macromolecules*, 2000, **33**, 3042-3049.
23. M. Mayer, J. Yang, I. Gitlin, D. H. Gracias and G. M. Whitesides, *PROTEOMICS*, 2004, **4**, 2366-2376.
24. S. Takeuchi, W. R. DiLuzio, D. B. Weibel and G. M. Whitesides, *Nano Letters*, 2005, **5**, 1819-1823.
25. T. Baba, T. Ara, M. Hasegawa, Y. Takai, Y. Okumura, M. Baba, K. A. Datsenko, M. Tomita, B. L. Wanner and H. Mori, *Molecular Systems Biology*, 2006, -.
26. E. H. Wintermute and P. A. Silver, *Molecular Systems Biology*, 2010, **6**, -.
27. K. D. Young, *Annual Review of Microbiology*, 2010, **64**, 223-240.
28. E. H. Wintermute and P. A. Silver, *Molecular Systems Biology*, 2010, **6**, 1-7.
29. H. J. Kim, J. Q. Boedicker, J. W. Choi and R. F. Ismagilov, *Proceedings of the National Academy of Sciences of the United States of America*, 2008, **105**, 18188-18193.
30. S. T. Flickinger, M. F. Copeland, E. M. Downes, A. T. Braasch, H. H. Tuson, Y. J. Eun and D. B. Weibel, *Journal of the American Chemical Society*, 2011, **133**, 5966-5975.
31. J. L. Connell, A. K. Wessel, M. R. Parsek, A. D. Ellington, M. Whiteley and J. B. Shear, *mBio*, 2010, **1**, e00202-00210.
32. S. T. Flickinger, M. F. Copeland, E. M. Downes, A. T. Braasch, H. H. Tuson, Y.-J. Eun and D. B. Weibel, *Journal of the American Chemical Society*, 2011, **133**, 5966-5975.

Supplementary Information (SI)

The single-cell chemostat: an agarose-based, microfluidic device for high-throughput, single-cell studies of bacteria and bacterial communities

Supplementary Discussion

Production-Diffusion Model for the Concentration Gradient Created by a Linear Colony

To better understand the proximity-dependent growth rates observed in Figure 5, we consider here a simple model for the metabolite concentration profile produced by a linear colony. We assume, for simplicity, that the production rate per unit length of the colony—the number of metabolite molecules excreted per unit time per unit length—η, is uniform. Moreover, we neglect the complicated effects of buffer flow through the gutters and assume only that removal of metabolite by buffer flow allows the system to relax to a steady state. Finally, we neglect the reflecting boundary condition of the glass coverslip. To first order, the effect of metabolite removal by the gutters and the glass coverslip will be to simply rescale the effective production rate of the colony, η. More detailed calculations, beyond the scope of current work, would be required to extract this parameter from our data.

At steady-state, the concentration, $c'(x,y)$, of the metabolite excreted by an infinitesimal length of a line source, dl, centered at the origin is governed by

$$D\nabla^2 c'(x,y) = -\eta\, dl\, \delta(\vec{r})$$

where D is the diffusion constant for the excreted metabolite. The solution of this expression is

$$c'(x,y) = \frac{\eta}{4\pi D}\frac{dl}{\sqrt{x^2+y^2}}.$$

The total concentration produced by a linear colony of length L centered at the origin and oriented along the x-axis is the integral over all infinitesimal line segments:

$$c(x,y) = \frac{\eta}{4\pi D}\int_{-L/2}^{L/2}\frac{1}{\sqrt{(x-l)^2+y^2}}dl = \frac{\eta}{4\pi D}\left[\sinh^{-1}\left(\frac{L-2x}{2y}\right)-\sinh^{-1}\left(-\frac{L+2x}{2y}\right)\right]$$

where l is the position of an infinitesimal point charge along the linear colony.

To further simplify our analysis, we approximate the concentration observed by a linear colony of the complementary auxotroph at some distance *y* from the metabolite source by the concentration at the center of that colony, i.e. $x = 0$. Thus,

$$c(0, y) = \frac{\eta}{2\pi D}\left[\operatorname{csch}^{-1}\left(\frac{2y}{L}\right)\right].$$

For all of the complementation experiments reported here, the observed growth rates for the auxotrophs are smaller than that observed when the needed amino acids are added, indicating that the excreted metabolite is limiting for growth. Thus, we expect the growth rate of the auxotroph to be approximately linear in the concentration of the needed metabolite, i.e. $g(y) = \gamma c(y)$. In addition, because we do not observe colonies separated by distances larger than our field of view, 100 μm, we expect to observe an average background growth rate, g_0, that is due to the average metabolite concentration produced by these unobserved, distant colonies. Thus, under our simplifying assumptions, we expect a proximity-dependent growth rate of

$$g(y) = a\left[\operatorname{csch}^{-1}\left(\frac{2y}{L}\right)\right] + g_0$$

where the coefficient contains the production rate, diffusion constant, and proportionality constant between growth rate and metabolite concentration: $a = \gamma \frac{\eta}{2\pi D}$.

Supplementary Figures

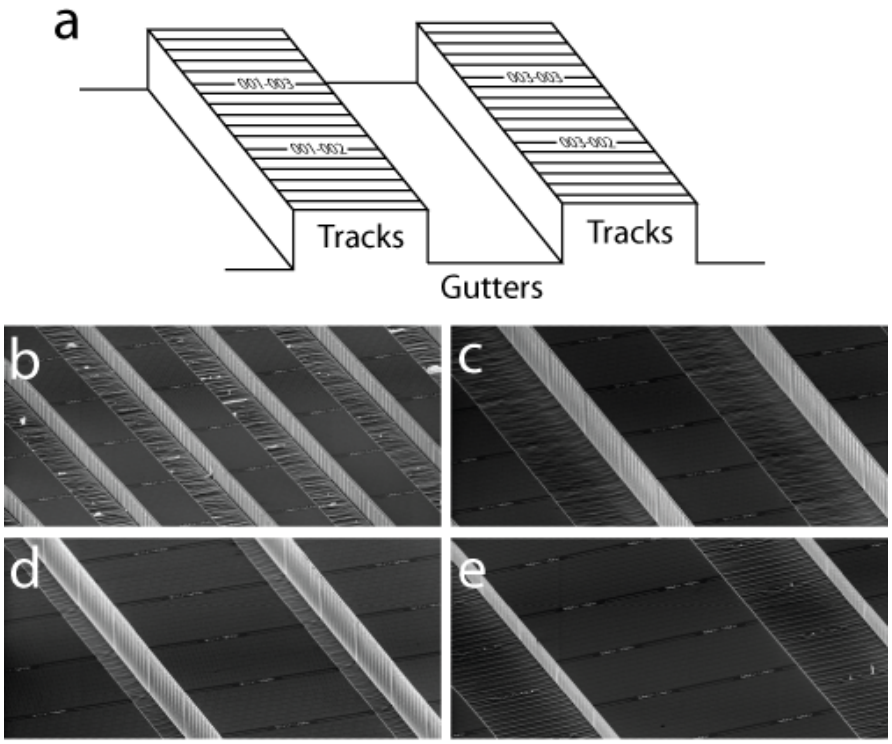

Figure S1: Views of different silicon masters. (a) Schematic diagram of the angled view of the silicon master pictured in this figure. (b)-(e) SEM images of silicon masters with (b) 50-µm long tracks and 50-µm wide by 20-µm deep gutters, (c) 100-µm long tracks with 100-µm wide by 40-µm deep gutters, (d) 150-µm long tracks with 50-µm wide by 40-µm deep gutters, and (e) 200-µm long tracks with 100-µm wide by 20-µm deep gutters. The 50-µm long tracks were printed with shallower gutters because agarose features with aspect ratios larger than ~0.5 (height to width) are easily damaged. The same shallow gutters were used with the 200-µm long tracks because the 50-µm and 200-µm long tracks were fabricated on the same silicon wafer. Images were collected with a 65 degree tilt from perpendicular, and all images share the same scale. *E. coli* has been successfully cultivated on patterned agarose with tracks 1.5-µm deep, 500 – 700-nm wide, and with each of the lengths pictured here (data not shown).

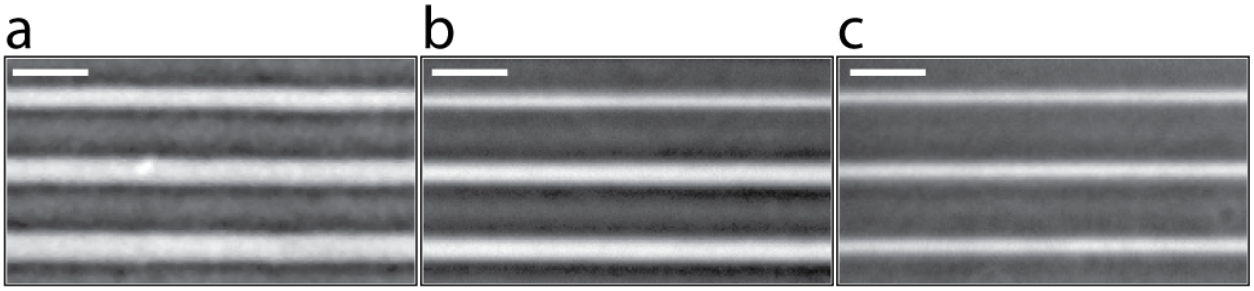

Figure S2: Patterned tracks of different widths. (a)-(c) Phase contrast images of patterned agarose gels (5% w/v) created with tracks decreasing in width from 1.0 µm (bottom of panel a) to 300 nm (top of panel c.) Gels created from silicon masters that (a) were not coated with SiO_2 or are coated with layers (b) 200 nm or (c) 400 nm thick. Tracks increase in width by approximately 100 nm from top to bottom in each image. Scale bars correspond to 2 µm, the smallest width previously printed into agarose. All pictured tracks are 1.5-µm deep though we have also printed tracks of the same width with depths of 1.25 µm and 1.0 µm (data not shown.)

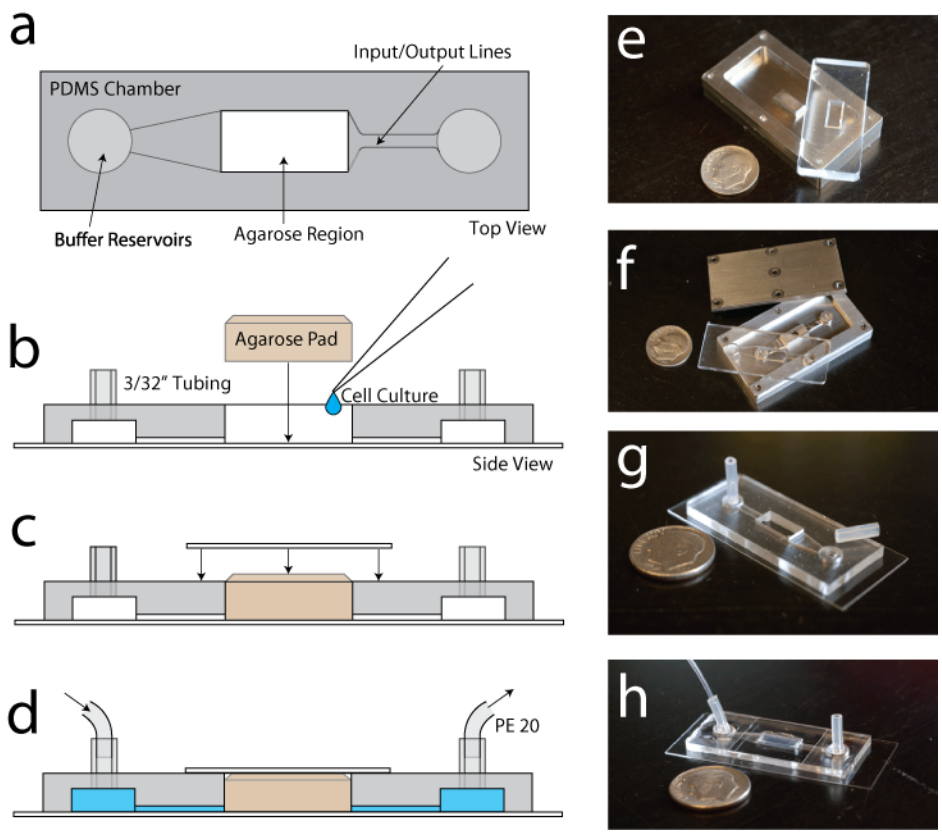

Figure S3: Experiment assembly. (a) Top view of the PDMS sidewall. (b) Side view of a partially assembled chamber. The bottom cover glass and the Tygon tubing have been added to create a chamber ready for cells and the printed pad. (c) Once the cells and the pad are loaded, an additional cover glass compresses and seals the device. (d) PE tubing is then used to introduce and remove buffer. (e) A PDMS gel mold and the stainless steel mold used to fabricate it. (f) A PMDS sidewall with the stainless steel mold used to create it. (g) A partially assembled chamber with Tygon tubing. (h) A fully assembled chamber with top cover slip and pad.

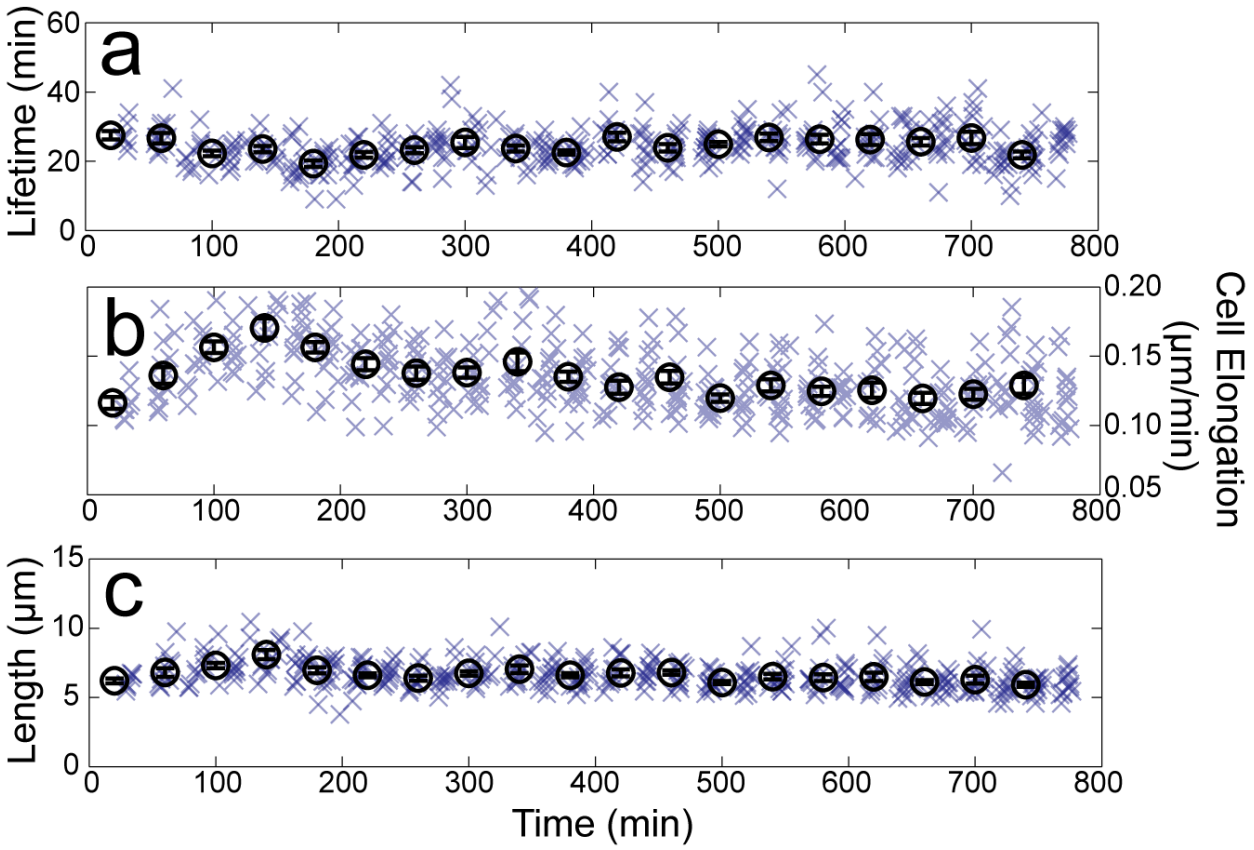

Figure S4: Growth properties of individual cells reveal a chemostatic environment. (a) Lifetime (or cell division time), (b) average cell elongation rate, and (c) length at division for all cells growing in the colony presented in Figure 2 and for which the initial and final division was observed. Average growth properties for individual cells (purple crosses) are plotted at times corresponding to the middle of the life of each cell. Averages (black circles) are computed over all cells within a 40-minute window, and error bars represent the standard error of the mean. Fluctuations in the average growth properties do not correlate between adjacent colonies (data not shown), revealing that these fluctuations are of biological origin.

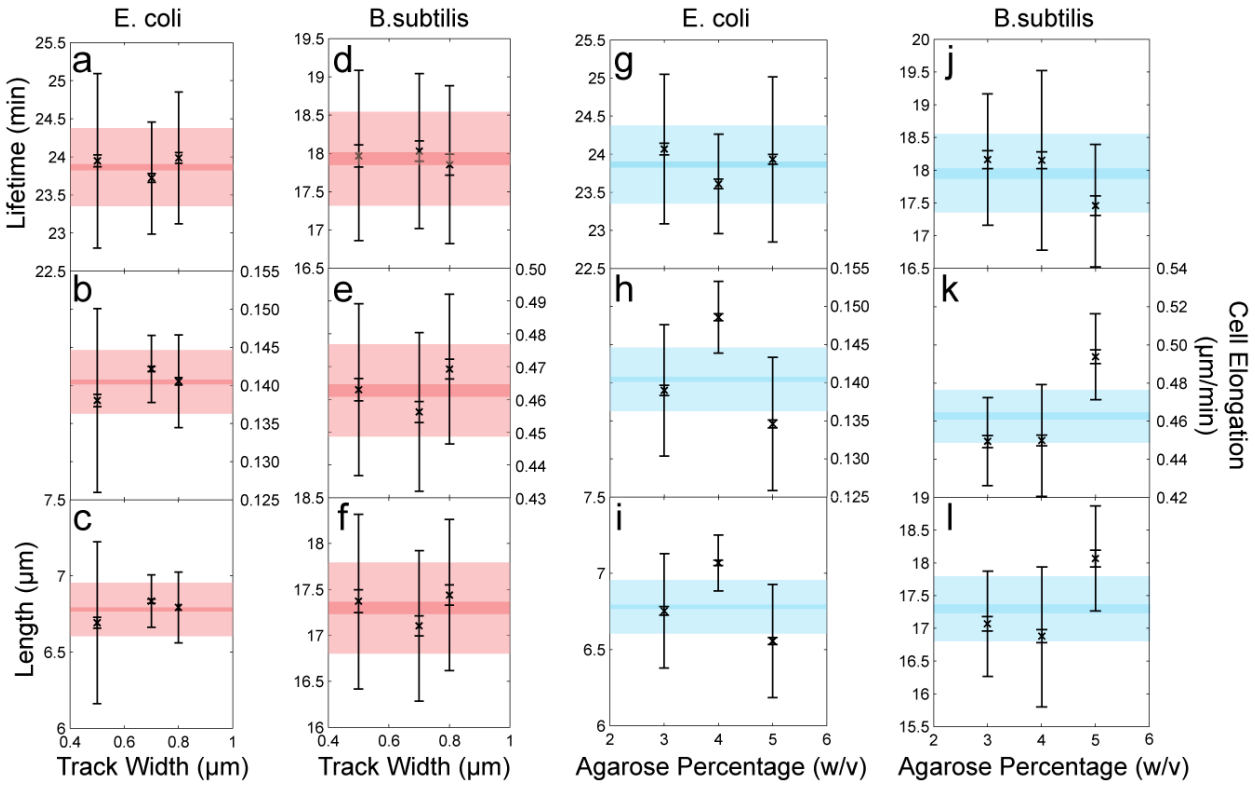

Figure S5: Growth does not vary with track width or agarose percentage. (a) Average lifetime, (b) cell elongation rate, and (c) length at division for *E. coli* growing in tracks of different widths. (d)-(f) The same growth properties for *B. subtilis* as a function of track width. All experiments were conducted with 1.5-μm deep tracks. In the rich medium of these experiments, *E. coli* has a diameter of ~0.8 μm, and *B. subtilis* has a diameter of ~1.0 μm; thus, most tracks are narrower but deeper than cells. (g-i) *E. coli* and (j-l) *B. subtilis* growth properties as a function of agarose percentage (w/v). Increasing the agarose percentage produces gels that are stiffer and, thus, exert more pressure on the cells. Black symbols represent the mean of all measured cells. The smaller error bars represent the standard error of the mean with respect to the number of cells while the larger error bars represent the standard error with respect to the number of clonal replicates, i.e. the number of colonies. The shaded regions are centered on the global mean, and the inner and outer regions correspond to the two standard errors of this global mean. No systematic trend with track width or agarose percentage is observed for any of the growth properties, indicating that the pressure applied by the tracks does not perturb the growth of either of these bacteria.

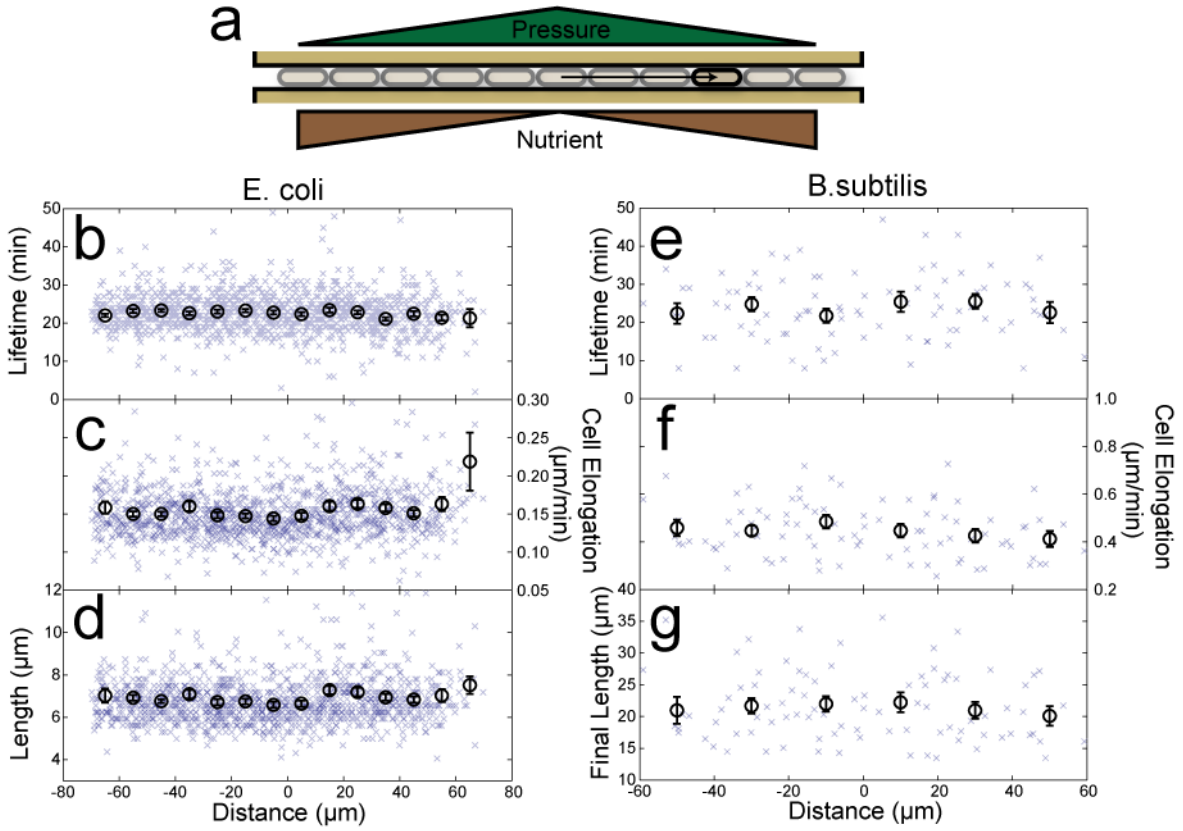

Figure S6: Growth does not vary with position in track. (a) Cartoon representation of the potential perturbations experienced by cells based on their position within the tracks. Near the center of the colonies, cells must generate the pressure required to push cells out of the colony. In addition, cells near the center are further from the nutrient source in the gutters and potentially observe a different nutrient environment. Both perturbations would predict that cells towards the center of the colony would grow more slowly than cells near the ends of the tracks. (b) Lifetime, (c) average cell elongation rate, and (d) length at division for *E. coli* growing in a 200-μm long colony as a function of distance from the average position of the source during the life of each cell. 200-μm long tracks were used to accentuate any potential position dependence. Distance is defined from the central stationary position in the colony (Fig. 2e), which typically is within ~10 μm of the geometric center of the colony. (e) Lifetime, (f) average cell elongation rate, and (g) length at division for *B. subtilis* growing in a 200-μm-long colony. Individual crosses represent the values for distinct cells while the circles represent the average for all cells in a 10-μm (*E. coli*) or 20-μm (*B. subtilis*) window. Error bars represent the standard error of the mean. No systematic trend as a function of length is observed, indicating that i) the pressure required to push out daughter cells does not perturb growth and ii) nutrient is supplied uniformly to all cells, even cells 100 μm from the gutters.

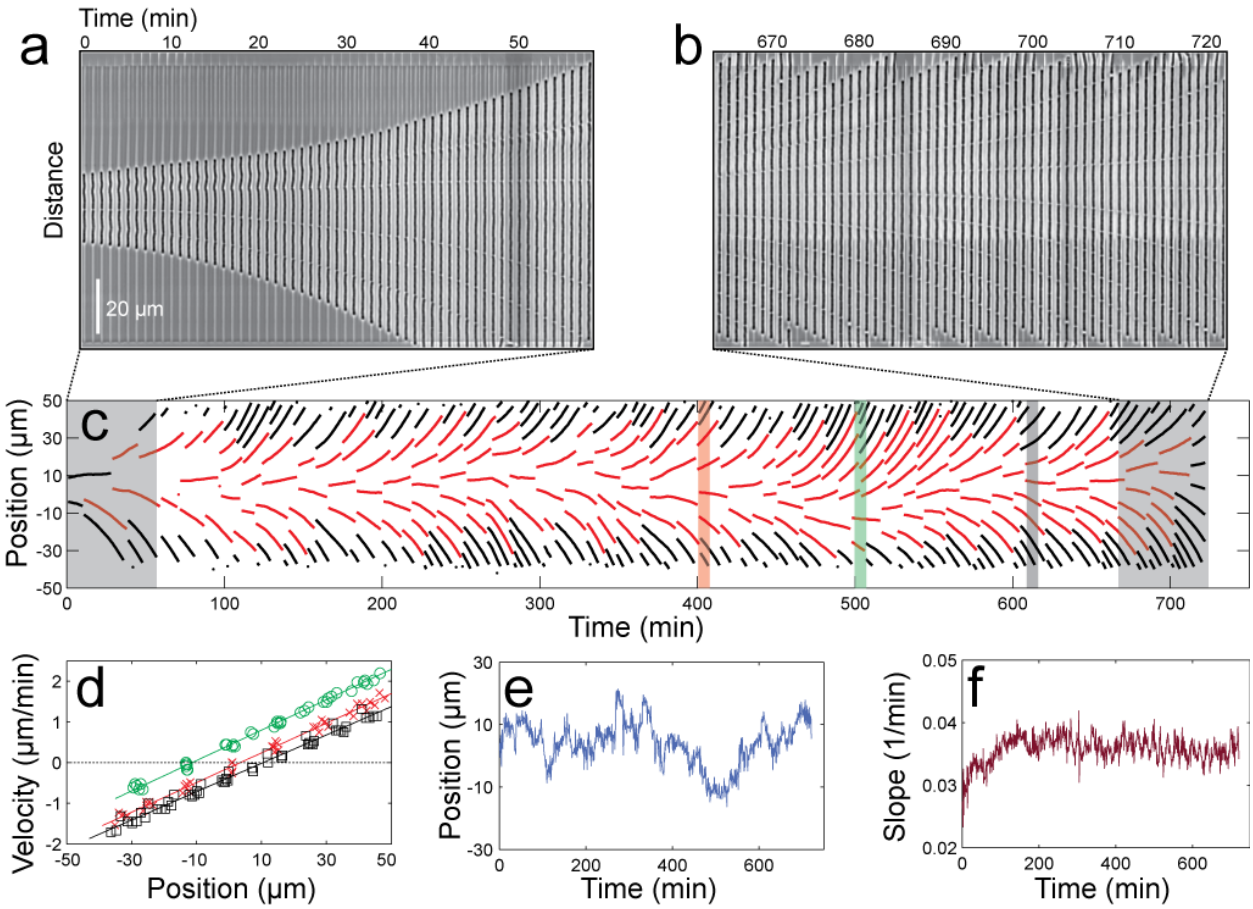

Figure S7: Growth dynamics of *B. subtilis*. (a) A kymograph-like image of a single *B. subtilis* colony growing at 35C in LB showing the first hour of growth after plating on the structured agarose pad. (b) A kymograph-like image of the same colony 12 hours later, showing that the morphology of the cells is identical to the morphology observed at the beginning of the measurement. (c) The position of each cell within the colony as a function of time. Red lines correspond to cells for which the initial and finial division have been observed, and black lines correspond to cells for which one of the divisions was not observed. (d) Center velocity as a function of position for cells at different times. Data are collected from 5-minute windows indicated by the similarly colored regions pictured in (b). Solid lines represent linear fits. (e) Stationary position within the colony as a function of time. Motion of this position indicates that cells can move freely within the track. (f) Expansion rate of the colony (slope of lines in panel (d)) as a function of time. After an initial response to being transferred to the device, the *B. subtilis* colony grows at a constant rate. Nearly 40 generations were observed under chemostatic conditions in this measurement.

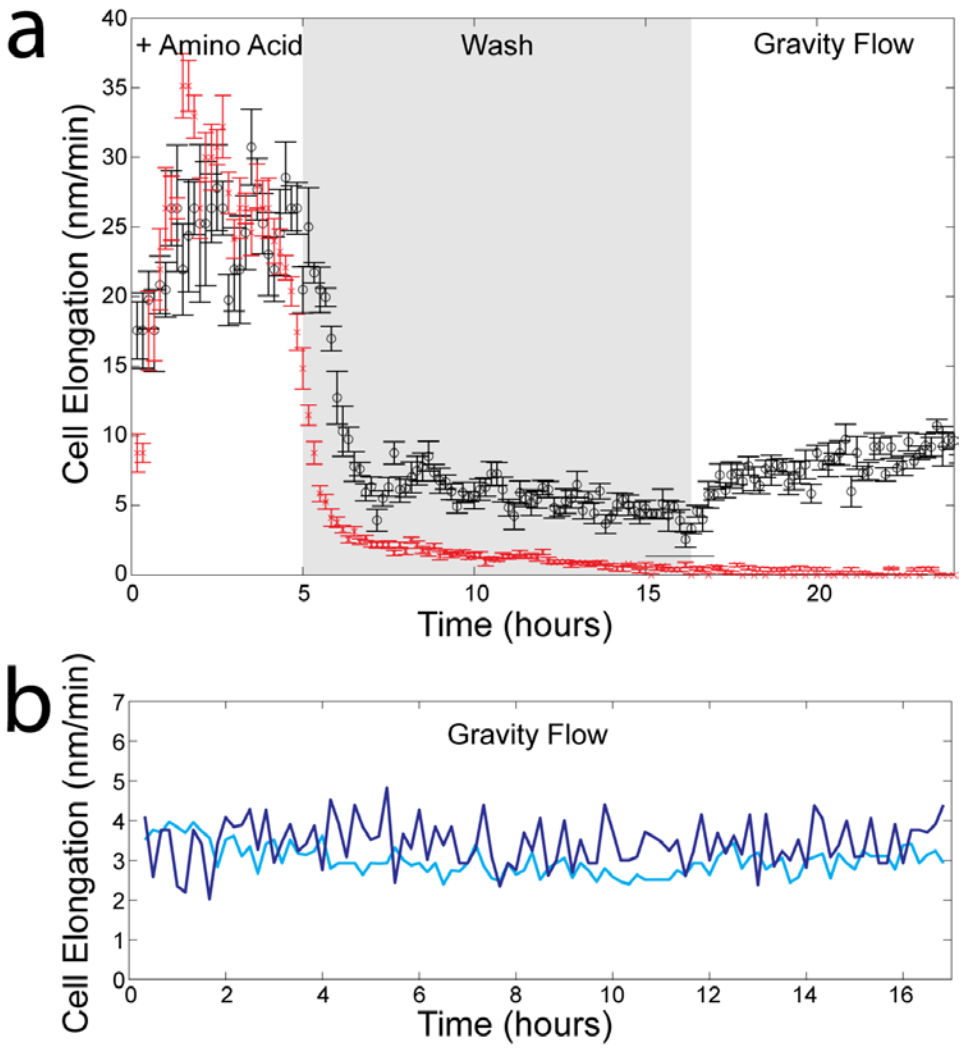

Figure S8: Preparation and chemostatic growth of a microbial community. (a) The median cell elongation rate for all cells during the preparation of a microbial community. Black corresponds to the growth of ΔilvE when equal numbers of ΔargC are present while red corresponds to the control experiment when ΔilvE is alone. Error bars correspond to the standard error of the mean. During the first 5 hours, the presence of amino acids dissolved into the gel (10 µM isoleucine, leucine, valine, and arginine) allows the auxotrophs to grow and fill the tracks. There is no flow during this period. Once growth has established the community, residual amino acid is removed by flowing minimal medium with glucose but without amino acids through the gutters at 10 µL/min. 12 hours of wash is required to reduce the growth of each auxotroph alone to background levels. After the wash step, the flow rate is changed, and the communication in the colony is allowed to equilibrate for 3 hours. A variety of flow rates have been used during this period; depicted here is gravity flow, in which a pressure difference between the buffer reservoir and the waste reservoir, due to a height difference, produces a slow flow (< 1 µL/min) that clears the gutters and provides nutrient. (b) The median cell elongation rate for ΔilvE (cyan) and ΔargC (blue) cells for 17 hours after the completion of the wash step in a community composed of 1/10 ΔargC.

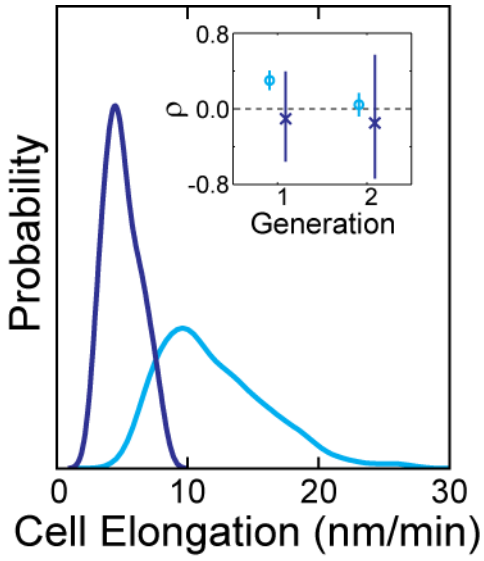

Figure S9: Growth within the community is homogeneous. Probability distributions for the average cell elongation rate of individual ΔilvE (cyan) and ΔargC (blue) cells calculated with kernel density estimation and the optimal kernel. Data are taken from a community of equal numbers of the two strains. Inset: Spearmen correlation coefficient for the inter-generational correlation of the average elongation rate between mothers and daughters (generation 1) and mothers and grand-daughters (generation 2). Bars correspond to 95% confidence intervals. To correct for colony-to-colony variations in growth rate, cells were ranked within colonies, and then the Pearson correlation coefficient was calculated for these ranks.

Supporting Movie Captions

Supporting Movie S1: Growth of *E. coli* in rich medium. Phase contrast time-lapse movie of *E. coli*, MG1655, growing in tracks 1.5-µm deep, 0.6 – 0.8-µm wide, and 100-µm long in 5% w/v agarose with rich defined medium at 35C. The frame rate is 1 per minute, and the entire movie runs for 4 hours.

Supporting Movie S2: **Growth of *E. coli* in minimal medium with glucose.** Phase contrast time-lapse movie of *E. coli*, MG1655, growing in tracks 1.5-µm deep, 0.6 – 0.8-µm wide, and 100-µm long in 4% w/v agarose with minimal defined medium and glucose at 35C. The frame rate is 1 per minute, and the movie runs for 4 hours.

Supporting Movie S3: **Growth of *E. coli* in minimal medium with glycerol.** Phase contrast time-lapse movie of *E. coli*, MG1655, growing in tracks 1.5-µm deep, 0.6 – 0.8-µm wide, and 100-µm long in 4% w/v agarose with minimal defined medium and glycerol at 35C. The frame rate is 1 per 4 minutes, and the movie runs for 4 hours.

Supporting Movie S4: Growth of *B. subtilis* in rich medium. Phase contrast time-lapse movie of *B. subtilis*, 3610, growing in tracks 1.5-µm deep, 0.6 – 0.8-µm wide, and 100-µm long in 5% w/v agarose with LB at 35C. The frame rate is 1 per minute, and the movie runs for 4 hours.

Supporting Movie S5: Growth of *E. faecalis* in rich medium. Phase contrast time-lapse movie of *E. feacalis*, E1sol, growing in tracks 1.5-µm deep, 0.6 – 0.8-µm wide, and 50-µm long in 4% w/v agarose with BHI at 35C. The frame rate is 1 per minute, and the movie runs for 3 hours.

Supporting Movie S6: Community growth of *E. coli* prototroph and ΔilvE. Phase contrast time-lapse movie of microbial community consisting of wild type *E. coli* and the *E. coli* auxotroph ΔilvE growing in 1.0-µm deep, 0.3-0.6-µm wide, and 50-µm long tracks in 4.5% w/v agarose with minimal defined medium and glucose at 35C. The frame rate is 1 per 5 minutes, and the movie contains 6 hours of a 24 hour measurement. Despite the dramatic difference in growth rate, wild type *E. coli* (faster growing colonies) are incapable of crowding the slowly growing auxotroph, permitting the long-term study of the interactions between these two strains.